Title: Homeostatic plasticity rules control the wiring of axo-axonic synapses at the axon initial segment

Authors: Alejandro Pan-Vazquez [1,2]†, Winnie Wefelmeyer [1,2]†, Victoria Gonzalez Sabater[1,2], Juan Burrone [1,2] *

Affiliations:

[1] MRC Centre for Neurodevelopmental Disorders, Institute of Psychiatry, Psychology and Neuroscience, King's College London, London, United Kingdom SE1 1UL

[2] Centre for Developmental Neurobiology, Institute of Psychiatry, Psychology and Neuroscience, King's College London, London, United Kingdom SE1 1UL

*Correspondence to: juan.burrone@kcl.ac.uk

† Equal contribution

Abstract: The activity-dependent rules that govern the wiring of GABAergic interneurons are not well understood. Chandelier cells (ChCs), a GABAergic interneuron, control pyramidal cell output through axo-axonic synapses that target the axon initial segment. *In vivo* imaging of ChCs during development uncovered a narrow window (P12-P18) over which axons arborized and formed connections. We found that increases in the activity of either pyramidal cells or individual ChCs during this temporal window results in a reversible decrease in axo-axonic connections, at a time when they are depolarising. Identical manipulations of network activity in older mice (P40-P46), when ChC synapses are inhibitory, resulted in an increase in axo-axonic synapses. We propose that the direction of ChC plasticity follows homeostatic rules that depend on the polarity of axo-axonic synapses.

One Sentence Summary: Axo-axonic synapse plasticity follows the developmental switch in polarity of GABAergic synaptic transmission.

Main Text: Homeostatic forms of plasticity are thought to play a central role in stabilising the overall activity levels of neuronal circuits in the brain (*1, 2*). Although GABAergic interneurons directly modulate ongoing circuit activity through local connections (*3*), the rules that drive the plasticity of GABAergic synapses are not well understood (*4, 5*). This question is all the more important in the context of brain development, where GABA released from interneurons switches polarity with age, transitioning from excitation to inhibition during circuit wiring (*6*). Understanding the rules that drive interneuron plasticity will not only shed light on how GABAergic synapses modulate local networks, but also on how circuits in the brain remain stable over time.

Chandelier cells (ChCs) comprise a well-defined class of fast-spiking GABAergic interneurons with axonal arbours that are ideally placed to control neuronal and circuit activity in the cortex (*7, 8*). Abnormalities in axo-axonic connections between ChCs and pyramidal neurons have been associated with developmental brain disorders such as schizophrenia (*9*) and epilepsy (*10, 11*), but the normal wiring mechanisms of these contacts remain unknown. We used a transgenic mouse line (Nkx2.1^{CreERT2}) (*12*) crossed with a reporter line (Ai9) to image the development of ChC axons in layer 2/3 of the somatosensory cortex *in vivo* (Fig. 1A). In line with the late arrival of ChCs to the cortex, *in vivo* imaging of individual ChCs over many days also showed a delayed period of axonal growth that peaked within a narrow window across different cells, from P12 to P18. More surprising was the fact that the axonal arbours of individual ChCs showed a rapid transition in their morphology, generally within two days, from an immature state with few cartridges, to a highly complex arbour with multiple cartridges that span a well-defined cortical domain (Fig. 1, B and C). The dendrites, on the other hand, appear to develop earlier and remain largely unchanged throughout this period. Mirroring the rapid growth of the axonal arbour, the number of

postsynaptic pyramidal cells contacted by an individual ChC also increased during this window (Fig. 1, D and E). Although we saw no change in the length of the AIS of pyramidal neurons throughout this developmental period (Fig. 1I), we did observe an abrupt increase in the number of synapses formed onto an AIS (Fig. 1 F to H) that matched the increase in axon arbour size. In agreement with these morphological findings, we also saw a functional increase in the amplitude (Fig. 1J) of IPSCs recorded from pyramidal cells in response to optogenetic stimulation of ChCs (Fig. S1) during the period of synaptogenesis, as well as a maturation of the intrinsic firing properties of ChCs (Fig. S2). We conclude that there is a narrow developmental window (P12-P18) over which ChCs connect to neighbouring pyramidal cells and establish a local microcircuit.

We next explored the role that network activity plays in the formation of ChC circuits in the somatosensory cortex. Using designer receptors exclusively activated by designer drugs (DREADDs - specifically hM3Dq) (*13*) expressed in layer 2/3 pyramidal neurons in the somatosensory cortex, we increased network activity during the window of ChC synaptogenesis by delivering the DREADD agonist, clozapine-N- oxide (CNO), from P12 to P18 (Fig. 2, A and B). This manipulation resulted in an increase in activity (verified by cFos expression) in both pyramidal cells that expressed hM3Dq and neighbouring cells that did not (referred to as hM3Dq-network), suggesting a network-wide increase in neuronal activity (Fig. 2B). Indeed, although increases in activity were initially confined exclusively to DREADD-expressing neurons (at P12; Fig. S3), activity spread to neighbouring neurons in the network by the end of the CNO treatment (at P18; Fig. 2B). We found that increased activity during this period resulted in a decrease in the overall number of pyramidal neurons contacted by a single ChC (Fig. 2C), a finding that highlights the role of activity in moulding the connectivity of inhibitory microcircuits. In parallel to this, the number of axo-axonic synapses formed by single ChCs decreased significantly in both pyramidal

neurons expressing DREADDs, as well as in neighbouring DREADD-negative (hM3Dq-network) pyramidal cells (Fig. 2 D to H), in agreement with a network-wide increase in activity (Fig. 2B). The connectivity between ChCs and pyramidal neurons was further studied functionally. IPSCs were recorded in pyramidal cells in response to optical stimulation of ChCs expressing channel-rhodopsin-2 (ChR2). Again, matching the morphological changes, we found that measures of connection strength, such as the amplitude of IPSCs and failure rates (Fig 2. I to L), as well as the connection probability (Fig. 2M) between ChCs and pyramidal neurons decreased in networks that were stimulated chemogenetically. We conclude that axo-axonic synapses are sensitive to network activity during this early period of synapse formation, decreasing their output in a hyperactive environment. Interestingly, basket cells, fast spiking interneurons that predominantly target the soma, showed an increase in the number of boutons onto hyperactive pyramidal cells (Fig. S4), suggesting differences in either the synaptic properties or the plasticity rules between interneuron subtypes during this period. Finally, measures of the structural properties of the AIS showed that DREADD-expressing pyramidal cells (but not neighbouring hM3Dq-network cells) tended to have shorter AISs (Fig. S5A), which were matched by a decrease in intrinsic excitability (Fig. S5B), a finding that is in line with homeostatic forms of plasticity previously observed at the axon initial segment in other systems (*14-18*). The confinement of AIS plasticity to DREADD-expressing neurons suggests that higher levels of activity are probably needed to drive this form of plasticity, which may only be achieved in those pyramidal cells directly activated by CNO.

The plasticity of both axo-axonic synapses and of the AIS were found to be reversible. Following six days of increased activity, mice were allowed to recover for a further five days without any CNO injections, after which axo-axonic synapse properties were assessed (Fig. 3A). All measures of axo-axonic synapse connectivity were found to recover back to normal levels, indistinguishable

from unstimulated neurons of the same age (Fig. 3 B to E). Surprisingly, although the length of the AIS also recovered, it grew beyond control levels (Fig. S6A), suggesting some kind of rebound effect during the recovery period. Together, our findings show that network activity reversibly controls the output of pyramidal cells during development by modulating both the structure of the AIS as well as the axo-axonic synapses that form onto it.

Increases in network activity are also likely to drive activity in ChCs through local intracortical connections (*19*). To establish if axo-axonic synapse plasticity requires the activity of pyramidal cells or can be driven by exclusively increasing the activity of ChCs in a cell-autonomous manner, we expressed DREADDs (hM3Dq) solely in ChCs (Fig. 3 F and G). Activation with CNO resulted in a similar reduction in synapse number and connection probability when compared to the plasticity driven by increases in pyramidal cell activity (Fig. 3 H to K). This manipulation did not result in any significant changes in the size of the AIS of pyramidal neurons (Fig. S6B). Our results are consistent with the idea that ChCs sample the ongoing levels of activity in local pyramidal cell circuits through changes in their own activity levels and alter their output accordingly.

The developing brain shows many forms of plasticity that are exclusive to early postnatal periods of brain wiring, that are not observed in adult circuits (*20, 21*). We therefore performed similar experiments to those above, but in older mice (Fig. 4A). Increasing the activity of cortical networks by delivery of CNO to DREADD (hM3Dq)-expressing pyramidal neurons from P40 to P46 did not cause a significant change in the number of postsynaptic pyramidal cells contacted by a single ChC (Fig. 4 B and C), nor did it recapitulate the decrease in axo-axonic synapse number observed during development. Instead, we observed an increase in synapses along the AIS (Fig. 4 D to F), without a significant change in the size of the AIS (Fig. S6C). This switch in the direction of axo-axonic synapse plasticity with age may be explained by a developmental change in the properties

of the synapses themselves. We therefore next probed the functional outcome of GABA released from axo-axonic synapses onto pyramidal cells.

In the context of homeostatic forms of plasticity that are thought to operate over these long timescales (*1, 22*), the decrease of ChC synapses in hyperactive networks during development (Fig. 2 A to K) is surprising and in clear contrast to both the increase in somatic GABAergic inputs in the same network (Fig. S4) and in older ChCs (Fig. 4 A to F). This discrepancy may be explained by recent work studying the switch in polarity of GABAergic synapses, as they transition from excitatory to inhibitory/shunting during development, along different subcellular compartments (*23*). Whereas GABAergic synapses on the somato-dendritic compartment switch polarity within the second postnatal week (*6*), those on the AIS remain depolarising well into the third postnatal week, providing a temporal window over which different interneurons could potentially drive pyramidal cell activity in opposite directions (*23*). We therefore explored the polarity of axo-axonic synapses at the AIS during this early period of synaptogenesis by performing voltage imaging of pyramidal neurons in acute slices obtained at P16-P18. This approach provided a readout of membrane potential responses to either local GABA iontophoresis or ChC stimulation without perturbation of the intracellular milieu. We first carried out local GABA iontophoresis at the AIS of pyramidal neurons expressing the genetically-encoded voltage indicator (GEVI) Ace-mNeon (*24*) (Fig. 4G; see Fig. S7 for voltage sensitivity). In agreement with previous findings (*18*), we found that GABA tended to produce strong depolarisations at the AIS that were sensitive to $GABA_A$ receptor antagonists (Fig. S8) during this developmental period (Fig. 4 H and I). To explore this further, we performed whole-cell patch clamping of ChCs to directly stimulate a single ChC and image voltage responses in neighbouring pyramidal cells that expressed Ace-mNeon (Fig. 4J). We found that clear responses could only be detected in 5 out of 27 recordings (Fig. 4 K

and L), a relatively low success rate which likely reflects a combination of functional connectivity (53% functional connection probability; see Fig. 1), coupled to a limited ability to measure subthreshold synaptic events. Nevertheless, all 5 measurable responses were depolarising (Fig. 4M). Our results strongly suggest that release of GABA by ChCs causes postsynaptic depolarisations in pyramidal neurons during the early period of synaptogenesis (P12-P18), in agreement with others (*23, 25-27*). Together with previous studies showing that ChCs decrease the activity of neighbouring pyramidal neurons in adult rodent brains (*19*), our findings have important implications for interpreting the plasticity of axo-axonic synapses described here. The switch in the plasticity of ChC outputs can be explained as a homeostatic response that depends on the polarity of the synapse at the time. Whereas in mature brains axo-axonic synapses are inhibitory and therefore respond to hyperactivity by increasing their number, early in development, when they are depolarising, they respond by decreasing their drive onto pyramidal cells. The direction of synaptic plasticity is therefore dependent on the polarity of axo-axonic synapses. Similarly, the opposite direction in the plasticity of axo-axonic versus axo-somatic synapses early in development is likely driven by the reversed polarity of each synapse type at the time.

Our results suggest that the wiring of GABAergic interneurons in the cortex is governed by homeostatic rules that control the number and strength of connections onto pyramidal cells. In this context, the plasticity of the AIS, together with its axo-axonic synapses, provide a hub for tightly modulating pyramidal cell activity, where multiple forms of plasticity come together in a concerted manner to stabilise the output of pyramidal neurons in the cortex.

References and Notes:

1. W. Wefelmeyer, C. J. Puhl, J. Burrone, Homeostatic Plasticity of Subcellular Neuronal Structures: From Inputs to Outputs. *Trends Neurosci* **39**, 656-667 (2016).
2. G. Turrigiano, Too many cooks? Intrinsic and synaptic homeostatic mechanisms in cortical circuit refinement. *Annu Rev Neurosci* **34**, 89-103 (2011).
3. A. Kepecs, G. Fishell, Interneuron cell types are fit to function. *Nature* **505**, 318-326 (2014).
4. N. V. De Marco Garcia, T. Karayannis, G. Fishell, Neuronal activity is required for the development of specific cortical interneuron subtypes. *Nature* **472**, 351-355 (2011).
5. T. Karayannis, N. V. De Marco Garcia, G. J. Fishell, Functional adaptation of cortical interneurons to attenuated activity is subtype-specific. *Frontiers in neural circuits* **6**, 66 (2012).
6. Y. Ben-Ari, J. L. Gaiarsa, R. Tyzio, R. Khazipov, GABA: a pioneer transmitter that excites immature neurons and generates primitive oscillations. *Physiol Rev* **87**, 1215-1284 (2007).
7. P. Somogyi, A specific 'axo-axonal' interneuron in the visual cortex of the rat. *Brain Res* **136**, 345-350 (1977).
8. M. Inan *et al.*, Dense and overlapping innervation of pyramidal neurons by chandelier cells. *The Journal of neuroscience : the official journal of the Society for Neuroscience* **33**, 1907-1914 (2013).
9. P. Fazzari *et al.*, Control of cortical GABA circuitry development by Nrg1 and ErbB4 signalling. *Nature* **464**, 1376-1380 (2010).
10. J. DeFelipe, Chandelier cells and epilepsy. *Brain* **122 (Pt 10)**, 1807-1822 (1999).

11. P. Marco, J. DeFelipe, Altered synaptic circuitry in the human temporal neocortex removed from epileptic patients. *Exp Brain Res* **114**, 1-10 (1997).

12. H. Taniguchi, J. Lu, Z. J. Huang, The spatial and temporal origin of chandelier cells in mouse neocortex. *Science* **339**, 70-74 (2013).

13. D. J. Urban, B. L. Roth, DREADDs (designer receptors exclusively activated by designer drugs): chemogenetic tools with therapeutic utility. *Annu Rev Pharmacol Toxicol* **55**, 399-417 (2015).

14. H. Kuba, Y. Oichi, H. Ohmori, Presynaptic activity regulates Na(+) channel distribution at the axon initial segment. *Nature* **465**, 1075-1078 (2010).

15. M. S. Grubb, J. Burrone, Activity-dependent relocation of the axon initial segment fine-tunes neuronal excitability. *Nature* **465**, 1070-1074 (2010).

16. M. D. Evans, A. S. Dumitrescu, D. L. H. Kruijssen, S. E. Taylor, M. S. Grubb, Rapid Modulation of Axon Initial Segment Length Influences Repetitive Spike Firing. *Cell Rep* **13**, 1233-1245 (2015).

17. W. Wefelmeyer, D. Cattaert, J. Burrone, Activity-dependent mismatch between axo-axonic synapses and the axon initial segment controls neuronal output. *Proceedings of the National Academy of Sciences of the United States of America* **112**, 9757-9762 (2015).

18. J. Muir, J. T. Kittler, Plasticity of GABAA receptor diffusion dynamics at the axon initial segment. *Front Cell Neurosci* **8**, 151 (2014).

19. J. Lu *et al.*, Selective inhibitory control of pyramidal neuron ensembles and cortical subnetworks by chandelier cells. *Nature neuroscience* **20**, 1377-1383 (2017).

20. D. H. Hubel, T. N. Wiesel, The period of susceptibility to the physiological effects of unilateral eye closure in kittens. *The Journal of physiology* **206**, 419-436 (1970).

21. L. C. Katz, C. J. Shatz, Synaptic activity and the construction of cortical circuits. *Science* **274**, 1133-1138 (1996).

22. G. G. Turrigiano, S. B. Nelson, Homeostatic plasticity in the developing nervous system. *Nature reviews. Neuroscience* **5**, 97-107 (2004).

23. G. Rinetti-Vargas, K. Phamluong, D. Ron, K. J. Bender, Periadolescent Maturation of GABAergic Hyperpolarization at the Axon Initial Segment. *Cell Rep* **20**, 21-29 (2017).

24. Y. Gong *et al.*, High-speed recording of neural spikes in awake mice and flies with a fluorescent voltage sensor. *Science* **350**, 1361-1366 (2015).

25. A. R. Woodruff *et al.*, State-dependent function of neocortical chandelier cells. *The Journal of neuroscience : the official journal of the Society for Neuroscience* **31**, 17872-17886 (2011).

26. A. Woodruff, Q. Xu, S. A. Anderson, R. Yuste, Depolarizing effect of neocortical chandelier neurons. *Frontiers in neural circuits* **3**, 15 (2009).

27. J. Szabadics *et al.*, Excitatory effect of GABAergic axo-axonic cells in cortical microcircuits. *Science* **311**, 233-235 (2006).

28. F. K. Wong *et al.*, Pyramidal cell regulation of interneuron survival sculpts cortical networks. *Nature* **557**, 668-673 (2018).

29. M. J. Krashes *et al.*, Rapid, reversible activation of AgRP neurons drives feeding behavior in mice. *J Clin Invest* **121**, 1424-1428 (2011).

30. E. Favuzzi *et al.*, Activity-Dependent Gating of Parvalbumin Interneuron Function by the Perineuronal Net Protein Brevican. *Neuron* **95**, 639-655 e610 (2017)

31. A. J. Hinojosa, R. Deogracias, B. Rico, The Microtubule Regulator NEK7 Coordinates the Wiring of Cortical Parvalbumin Interneurons. *Cell Rep* **24**, 1231-1242 (2018).

32. I. Del Pino *et al.*, Erbb4 deletion from fast-spiking interneurons causes schizophrenia-like phenotypes. *Neuron* **79**, 1152-1168 (2013).

33. J. S. Rothman, R. A. Silver, NeuroMatic: An Integrated Open-Source Software Toolkit for Acquisition, Analysis and Simulation of Electrophysiological Data. *Front Neuroinform* **12**, 14 (2018).

Acknowledgments: We would like to thank Matthew Grubb, Adil Kahn, Oscar Marin and Beatriz Rico for comments on the manuscript; Ruben Deogracias and Beatriz Rico for help with the virus injections; Varun Sreenivasan and Oscar Marin for help with 2-photon microscopy. **Funding:** This work was supported by a Wellcome Trust Investigator Award (095589/Z/11/Z) and an ERC Starter Grant (282047) to JB, as well as MRC studentships to APV and to VGS.

Author contributions: Conceptualization, APV, WW and JB; Methodology, APV, WW, VGS; Software, APV, WW and VGS; Formal analysis, APV, WW and VGS; Investigation, APV, WW; Writing-Original Draft, APV, WW and JB; Writing- Review & Editing, APV, WW and JB; Funding Acquisition, APV, VGS, JB; Supervision WW and JB. **Competing interests:** Authors declare no competing interests. **Data and materials availability:** All data is available upon request.

Supplementary Materials:

Materials and Methods

Figures S1-S8

References (*28-33*)

Fig. 1. Development of chandelier cells and axo-axonic synapses (A) Genetic strategy and timeline for tamoxifen injection for labelling ChCs in Nkx2.1$^{+/-}$CreERT2:Ai9 mice, implantation of cranial window and repeated *in vivo* imaging. **(B)** *In vivo* image (P16) and reconstructions (P12-P16) of a ChC. **(C)** Number of cartridges for individual ChCs (grey), mean cartridge number (black) and percentage change in cartridge number (red) during development (n=4 ChCs, 3 mice). **(D)** Image of a ChC (green) and AISs (red). Connection probability was measured within a 90 µm radius (white circle). 4-5 ChCs, 2-4 mice, per time-point. **(E)** Average connection probability of ChCs across development. **(F)** Images of axo-axonic synapses expressing VGAT on an AIS. **(G)** Average number and **(H)** density of axo-axonic boutons as well as **(I)** AIS length across development. Red lines in E,G,H and I represent a sigmoidal fit of the data. N=26-81 AISs, 2-4 mice per time-point. **(J)** ChCs expressing ChR2 were stimulated with light and IPSCs recorded in nearby pyramidal cells (left). Example responses (middle) and average IPSC amplitude (right) in immature and mature networks (**$p<0.01$, Mann-Whitney Test. N = 10-11 neurons, 4 mice, per condition). Bar plots show mean ± s.e.m.

Fig. 2. Activity-dependent plasticity of axo-axonic synapses. (A) Schematic of DREADD receptor hM3Dq (top left), timeline of CNO application (bottom left) and logic of experimental design resulting in hM3Dq+ (green) and hM3Dq- (grey) cells in the same network. **(B)** Representative images of cfos expression in L2/3 cells (left) following injections of CNO/saline P12-P18. Percentage of cfos positive cells across conditions (right) (Chi-Square test, N = 300 cells, 3 mice, per condition). **(C)** Connection probability of ChCs at P18 in a 90 and 180 µm radius

(dashed circles) (Chi-Square test. N=270-390 cells, 3-4 mice, per condition). **(D)** Example images showing axo-axonic boutons overlapping with the AIS. **(E-F)** Cumulative distribution of and average axo-axonic synapse density and number (One-way Kruskal-Wallis with Dunn's multiple comparison test. N=20-132 cells, 3-4 mice, per condition). **(G)** Example images of axo-axonic cartridges. **(H)** Cumulative distribution of and average cartridge size (Kruskal-Wallis with Dunn's multiple comparison test, N=21-40 neurons, 3-4 mice, per condition). **(I,J)** Representative IPSCs from pyramidal cells after optogenetic ChC stimulation for CNO control (blue) and hM3Dq-network (black) conditions. **(K)** Average IPSC amplitudes and **(L)** average IPSC failure rates (Chi-Square test, N=13-14 neurons, 4 mice, per condition). **(M)** Connection probability (Chi-Square test, N=36-57 neurons, 5 mice, per condition). Bar plots show mean ± s.e.m.

Fig. 3. Axo-axonic plasticity is reversible and cell-autonomous. (A) Logic of experimental design and timeline of CNO application. **(B)** Connection probability within a 90 µm radius at P22 (Chi-square test, N = 180-390 AISs from 2-3 mice, per condition). **(C)** Example images of axo-axonic synapses and AISs following the recovery period. **(D,E)** Cumulative distribution of and average axo-axonic synapse density and number (# denotes $p<0.05$, Kruskal Wallis test with Dunn's posthoc comparisons; ***$p<0.01$ for P18 versus P22 hM3Dq-network comparison tested with Mann-Whitney test. N = 41-89 neurons, from 2-3 mice, per condition. **(F)** Timeline of CNO delivery (top left) and strategy for viral delivery of GFP and hM3Dq to ChCs (bottom left). Experimental conditions of viral strategy (right). **(G)** Example images of P18 control and hM3Dq+ ChCs. **(H)** Connection probability within a 90 µm radius in control and hM3Dq+ ChCs, Chi-square test. N=120-150 AISs from 3 mice, per condition. **(I)** Example images of P18 CNO control and

hM3Dq+ cartridges. **(J,K)** Cumulative distribution of and average axo-axonic synapse density and number. Mann-Whitney test, N = 60 AISs from 3 mice, per condition.

Fig. 4. Axo-axonic plasticity matches GABAergic polarity. (A) Timeline for CNO delivery in adult mice. **(B,C)** Connection probability within a 90 µm radius at P46 (Chi-square test, N=150-180 AISs, 3-4 mice, per condition). **(D)** Example images of axo-axonic synapses in the different conditions. **(E,F)** Cumulative distribution and average axo-axonic synapse density and number (# denotes $p<0.05$ for one-way ANOVA without reaching significance in posthoc comparisons; *$p<0.05$ denotes Kruskal-Wallis and Dunn's posthoc comparisons test, N=44-72 neurons per condition, 3-5 mice, per condition. **(G)** Schematic showing iontophoresis experiments. Pipettes containing GABA are placed near the AIS of a pyramidal neuron expressing ACE-mNeon. **(H)** Epifluorescence images showing neurons expressing ACE-mNeon, the iontophoresis pipette at the AIS (white arrow) and corresponding $\Delta F/F$ traces. Fluorescence was measured at the soma (dashed circle). Left example cell shows a depolarising response to GABA application (grey area), right cell a hyperpolarising response. **(I)** Classification of responses into hyperpolarising (blue) and depolarising (red) for all cells tested. **(J)** Schematic showing experimental logic: ChCs were patch-clamped to evoke APs and responses were imaged from nearby pyramidal cells expressing ACE-mNeon. **(K)** Left, example image of ACE-mNeon cells, with somas outlined in different colours. Right, voltage imaging responses from corresponding cells following ChC stimulation (top; 5 APs, 50 Hz) (* denotes time-locked event 3x > baseline standard deviation). **(L)** Classification of all PSP responses obtained. Bar plots show mean ± s.e.m.

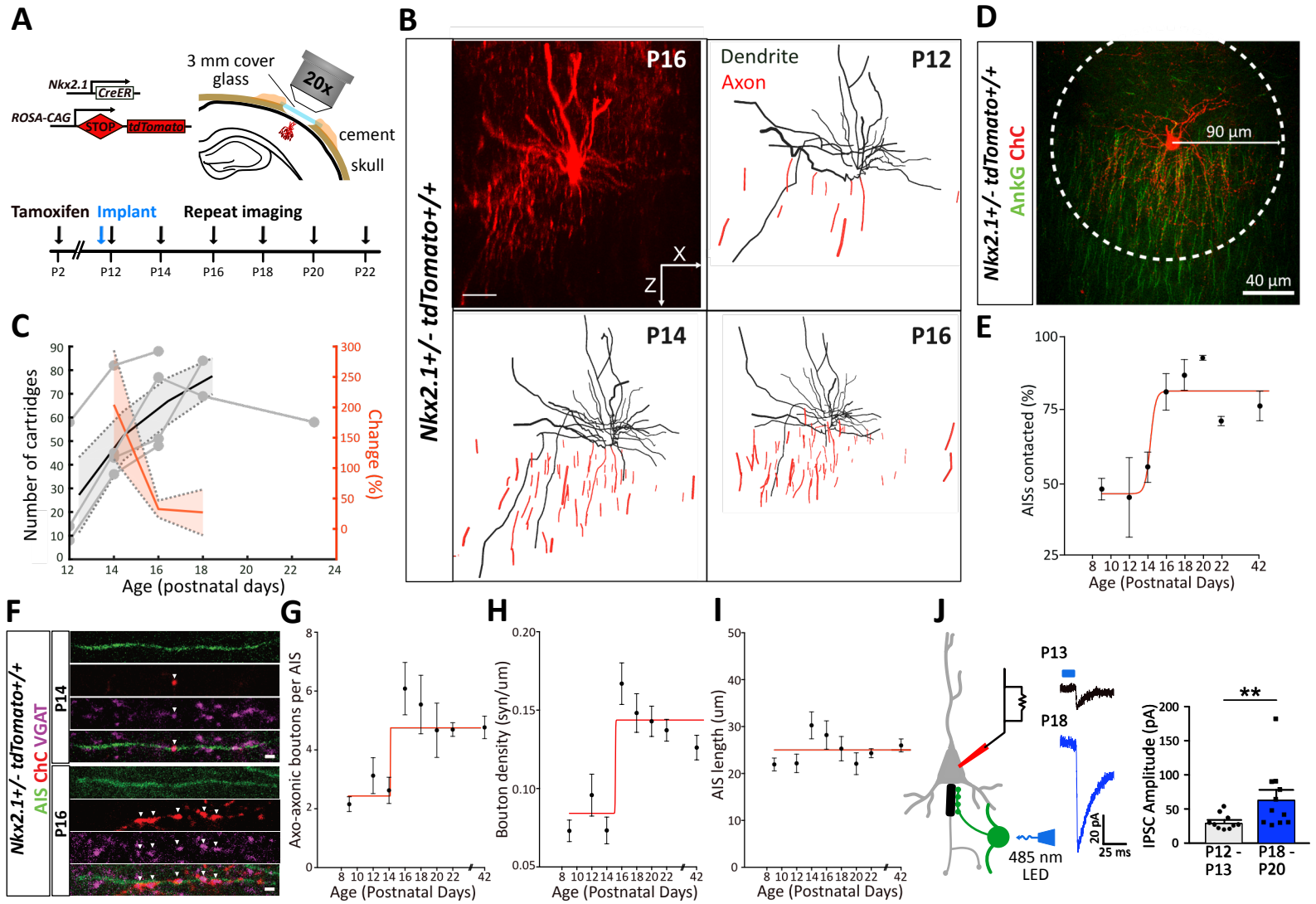
A
Nkx2.1
CreER
ROSA-CAG
STOP
tdTomato
3 mm cover glass
20x
cement
skull
Tamoxifen
Implant
Repeat imaging
P2
P12
P14
P16
P18
P20
P22
B
Nkx2.1+/- tdTomato+/+
P16
X
Z
Dendrite
Axon
P12
P14
P16
C
Number of cartridges
Change (%)
Age (postnatal days)
D
Nkx2.1+/- tdTomato+/+
AnkG ChC
90 µm
40 µm
E
AISs contacted (%)
Age (Postnatal Days)
F
Nkx2.1+/- tdTomato+/+
AIS ChC VGAT
P14
P16
G
Axo-axonic boutons per AIS
Age (Postnatal Days)
H
Bouton density (syn/um)
Age (Postnatal Days)
I
AIS length (um)
Age (Postnatal Days)
J
P13
P18
485 nm LED
20 pA
25 ms
IPSC Amplitude (pA)
**
P12 - P13
P18 - P20

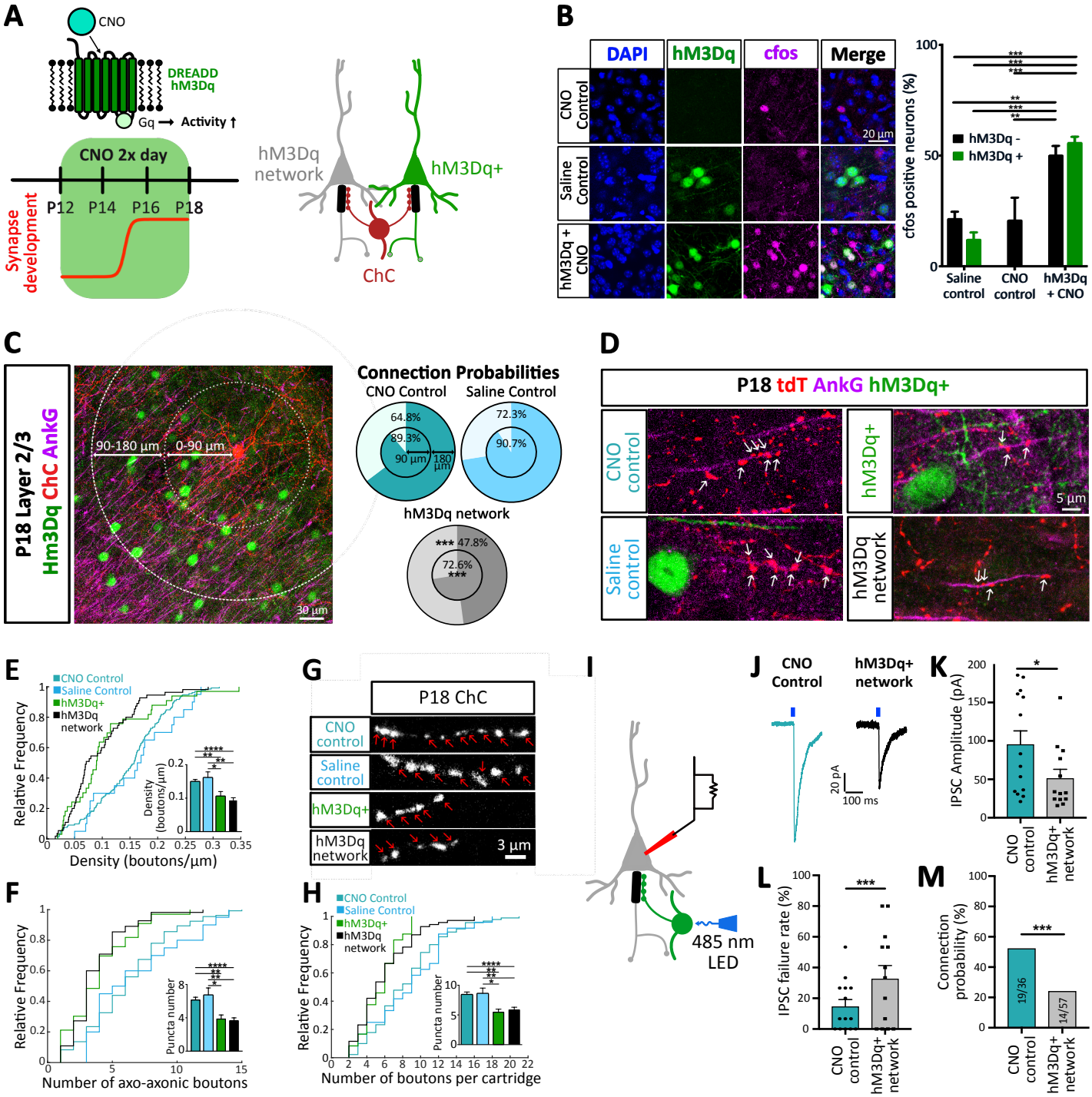
A
CNO
DREADD hM3Dq
Gq → Activity ↑
CNO 2x day
P12 P14 P16 P18
Synapse development
hM3Dq network
hM3Dq+
ChC
B
DAPI
hM3Dq
cfos
Merge
CNO Control
Saline Control
hM3Dq + CNO
20 µm
cfos positive neurons (%)
hM3Dq -
hM3Dq +
Saline control
CNO control
hM3Dq + CNO
C
P18 Layer 2/3
Hm3Dq ChC AnkG
90-180 µm
0-90 µm
30 µm
Connection Probabilities
CNO Control
Saline Control
64.8%
89.3%
90 µm
180 µm
72.3%
90.7%
hM3Dq network
47.8%
72.6%
D
P18 tdT AnkG hM3Dq+
CNO control
Saline control
hM3Dq+
hM3Dq network
5 µm
E
CNO Control
Saline Control
hM3Dq+
hM3Dq network
Relative Frequency
Density (boutons/µm)
F
Relative Frequency
Puncta number
Number of axo-axonic boutons
G
P18 ChC
CNO control
Saline control
hM3Dq+
hM3Dq network
3 µm
H
CNO Control
Saline Control
hM3Dq+
hM3Dq network
Relative Frequency
Puncta number
Number of boutons per cartridge
I
485 nm LED
J
CNO Control
hM3Dq+ network
20 pA
100 ms
K
IPSC Amplitude (pA)
CNO control
hM3Dq+ network
L
IPSC failure rate (%)
CNO control
hM3Dq+ network
M
Connection probability (%)
19/36
14/57
CNO control
hM3Dq+ network

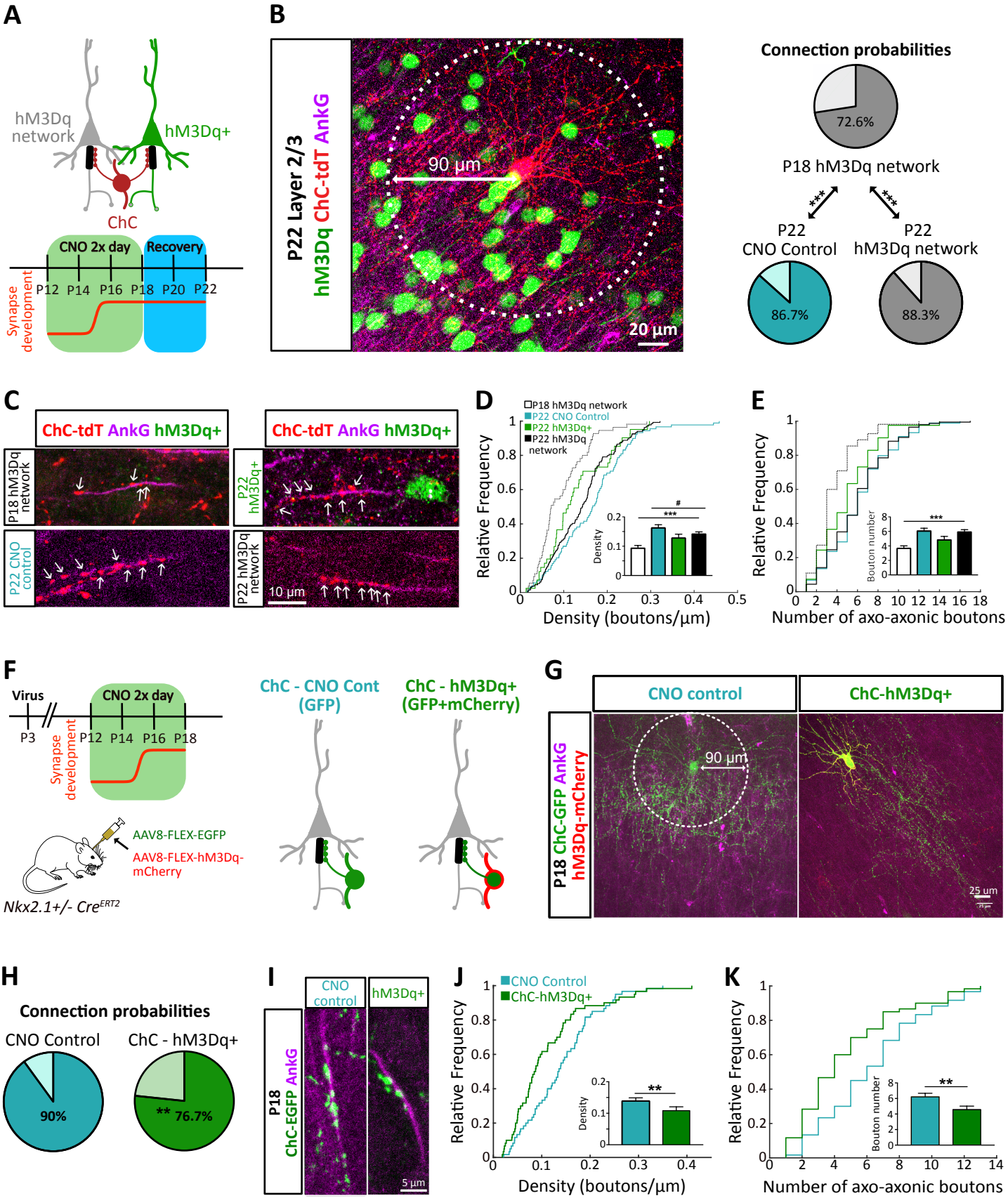
A
hM3Dq network
hM3Dq+
ChC
CNO 2x day
Recovery
P12 P14 P16 P18 P20 P22
Synapse development
B
P22 Layer 2/3
hM3Dq ChC-tdT AnkG
90 µm
20 µm
Connection probabilities
72.6%
P18 hM3Dq network
***
***
P22 CNO Control
P22 hM3Dq network
86.7%
88.3%
C
ChC-tdT AnkG hM3Dq+
ChC-tdT AnkG hM3Dq+
P18 hM3Dq network
P22 hM3Dq+
P22 CNO control
P22 hM3Dq network
10 µm
D
P18 hM3Dq network
P22 CNO Control
P22 hM3Dq+
P22 hM3Dq network
Relative Frequency
Density (boutons/µm)
Density
#
***
E
Relative Frequency
Number of axo-axonic boutons
Bouton number
***
F
Virus
CNO 2x day
P3
P12 P14 P16 P18
Synapse development
AAV8-FLEX-EGFP
AAV8-FLEX-hM3Dq-mCherry
Nkx2.1+/- CreERT2
ChC - CNO Cont (GFP)
ChC - hM3Dq+ (GFP+mCherry)
G
CNO control
ChC-hM3Dq+
P18 ChC-GFP AnkG hM3Dq-mCherry
90 µm
25 µm
H
Connection probabilities
CNO Control
ChC - hM3Dq+
90%
** 76.7%
I
CNO control
hM3Dq+
P18 ChC-EGFP AnkG
5 µm
J
CNO Control
ChC-hM3Dq+
Relative Frequency
Density (boutons/µm)
Density
**
K
Relative Frequency
Number of axo-axonic boutons
Bouton number
**

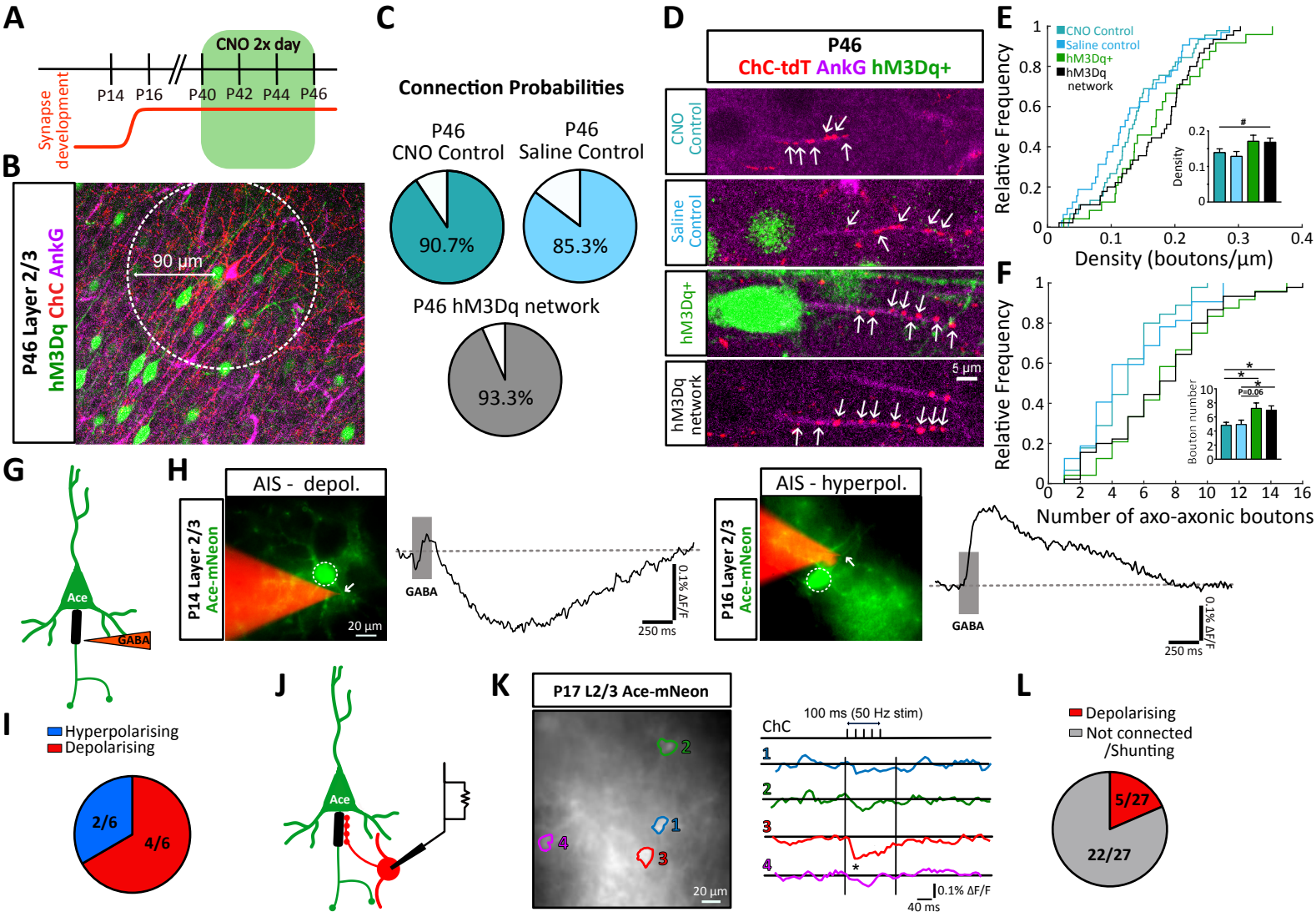
A
CNO 2x day
P14 P16 P40 P42 P44 P46
Synapse development
B
P46 Layer 2/3
hM3Dq ChC AnkG
90 µm
C
Connection Probabilities
P46 CNO Control
90.7%
P46 Saline Control
85.3%
P46 hM3Dq network
93.3%
D
P46
ChC-tdT AnkG hM3Dq+
CNO Control
Saline Control
hM3Dq+
hM3Dq network
5 µm
E
CNO Control
Saline control
hM3Dq+
hM3Dq network
Relative Frequency
Density (boutons/µm)
Density
F
Relative Frequency
Number of axo-axonic boutons
Bouton number
P=0.06
G
Ace
GABA
H
AIS - depol.
P14 Layer 2/3
Ace-mNeon
20 µm
GABA
0.1% ΔF/F
250 ms
AIS - hyperpol.
P16 Layer 2/3
Ace-mNeon
GABA
0.1% ΔF/F
250 ms
I
Hyperpolarising
Depolarising
2/6
4/6
J
Ace
K
P17 L2/3 Ace-mNeon
20 µm
ChC
100 ms (50 Hz stim)
0.1% ΔF/F
40 ms
L
Depolarising
Not connected /Shunting
5/27
22/27